The Institute of Space and Astronautical Science
Report SP No. 16, March 2003

Non-destructive three-dimensional analysis of MUSES-C samples by micro X-ray CT method using synchrotron radiation

By

Akira TSUCHIYAMA*, Tsukasa NAKANO† and Kentaro UESUGI‡

(1 February 2003)

Abstract: Two MUSES-C analog samples and a CM2 meteorite (the Murray meteorite) were imaged three-dimensionally without breaking the samples by an X-ray CT system at SPring-8 with the spatial resolution of about 10 μm. Based on the empirical relation between the CT-values, f, of materials in CT images and their X-ray linear attenuation coefficient, μ. ($f = 0.9\ \mu$), we estimated materials in the samples from their CT-values with the aid of image analysis technique (CBC-MS analysis). As the analog samples are fine powders, three-dimensional textures were not examined. High-resolution system (about 1 μm spatial resolution) at SPring-8 is useful for such samples. We can successfully recognize chondrules and mineral grains three-dimensionally in the Murray meteorite. The present method is useful to describe three-dimensional structures of unknown samples without breaking samples by using CT-values. We believe that curation of MUSES-C samples will be made effectively.

1. INTRODUCTION

X-ray computed tomography (CT) is a non-destructive method, which can obtain cross-sectional images of objects by using X-ray attenuation. In the CT images, the distribution of the contrasts shows the two-dimensional distribution of CT-values, which are related to X-ray linear attenuation coefficient (LAC) of objects. Three-dimensional structures of samples can be obtained by constructing a number of successive images. Using synchrotron radiation (SR) in the X-ray CT method gives following advantages. (1) High-quality images with high S/N ratio are obtained due to high flux density of X-ray photon. (2) Monochromatic X-ray beams can be available also due to the high flux density. Beam-hardening effect, which is appeared in conventional CT system using polychromatic X-ray beams, disappears and thus, quantitative relations between CT-values and LAC can be obtained. (3) Highly-collimated SR

* Department of Earth and Space Science, Graduate School of Science, Osaka University, 1-1 Machikaneyama-cho, Toyonaka, 560-0043 Japan. Electric mail: akira@ess.sci.Osaka-u.ac.jp
† Geological Survey of Japan/AIST, 1-1-1 Higashi, Tsukuba, 305-8567 Japan.
‡ SPring-8/JASRI, 1-1-1 Koto, Mikaduki, 679-5198 Japan.

beams can give three-dimensional structures easily although the size of a sample is limited. Lately, Uesugi et al. (1999) developed a new SR-CT system at SPring-8 in Japan. In this system, spatial resolution of CT images is regularly about 10 μm (sample size: < 5 μm). It is about 1 μm if small samples (< 0.5 μm) are imaged using a high spatial resolution detector system (Uesugi et al., 2000). If relation between CT-value and LAC is known, we can estimate materials by using LAC from their CT-values. The purpose of this study is to show that the SR-CT system is useful for MUSES-C samples. We expect that samples can be described three-dimensionally before distribution of the samples for detailed analysis (curation by X-ray CT method). Based on the results, we will make optimization for further analyses, for example by evaluating in heterogeneity of the samples and determination of cutting positions. In the present study, we imaged two MUSES-C analogue samples that were received from ISAS. Estimation of constituent materials and observation of three-dimensional internal structures were made. Before the imaging, we also imaged standard materials to obtain the relation between CT-values and LAC. A new image analysis for three-dimensional CT images was also developed for the material estimation.

2. RELATION BETWEEN CT- ANDd LAC-VALUES

About thirty standard materials including important rock-forming minerals, such as olivine, pyroxene, feldspar, quartz, troilite and metallic iron, were imaged at BL20B2 of SPring-8 using a two-dimensional X-ray detector, AA40MOD (Hamamatsu Photonics, K.K.), which is called as beam monitor-2 (BM2) with different photon energies, 20 to 70 keV. Histograms of CT-values were obtained from the three-dimensional images. By Gaussian fitting of each histogram peak corresponding to each standard material, we measured CT-values of the materials, f, and their deviations (the half-value widths), Δf. The LAC-values, μ , were calculated from the densities and chemical compositions of the materials as a function of photon energy (Tsuchiyama et al., 2000). The results show that the CT-value is proportional to the LAC, but slightly less than μ (Fig. 1):

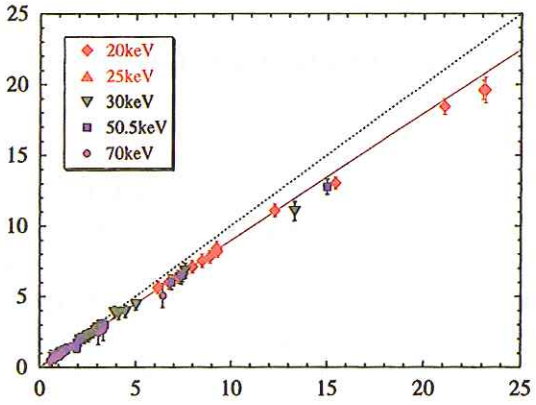

Fig. 1: CT values of standard materials, f, compared with calculated X-ray linear attenuation coefficient (LAC), μ, at different X-ray photon energies. A red line shows $f = 0.9\mu$

$$f = 0.9\mu. \tag{1}$$

We can determine LAC empirically from CT-values by using Eq.(1) although the cause of the factor of 0.9 has not been known at present. It should be also noted that Δf is approximately proportional to f at least at low photon energies (<30 keV):

$$\Delta f / f^{-0.1}. \tag{2}$$

3. IMAGING OF MUSES-C SAMPLES

We received two samples from ISAS, MUSES-C analog♯1 and analog♯2. Both are fine powders. Analog♯1 is dark gray in color, while analog♯2 is grayish white. The powdered samples were put into glass capillaries with outer and inner diameters of 1.2 and 0.8 mm, respectively. Imaging was made at BL20B2 using BM2 as in the case of standard material imaging. Two different photon energies were used for each sample; 25 and 30 keV for analog♯1 and 30 and 40 keV for analog♯2. It took about 2 to 6 hrs for taking X-ray projections images of each sample. It took about another 5 to 10 hours for reconstructing three-dimensional CT images. The pixel size of the slice images and slice width are 5.83 μm. Thus, the spatial resolution is about 10 μm or slightly poorer because an objet having two or three pixels can be recognized. We also imaged a bulk sample of a CM2 chondrite (the Murray meteorite) at 35 keV to test the CT method for a bulk sample. A piece of the meteorite (about 3–4 mm in size) was put onto a plastic tube (about 3 mm in outer diameter). We were able to fix the sample without any glue. So, we do not worry about contamination from glue.

Successive CT images of the samples are shown in Fig. 2 for the analog. About 900 slices were obtained for the three-dimensional structures. Typical images are shown in Fig. 3. In the CT images, objects with dark and bright contrasts (thus, low and high CT-values) have low and high attenuation of X-rays, respectively. CT images of the Murray meteorite are shown in Figs. 4 and 5. About 680 slices were obtained for the three-dimensional structure. Histograms of the CT-values were obtained from the three-dimensional CT images, in which the sample portions are masked. To show minor peaks or bumps as well as major peaks, logarithm of the number of voxels (imaging elements in a three-dimensional image like pixels in a two-dimensional image) is taken in the histograms ($\log(N)$-histogram) in Fig. 6 for the analog samples and Fig. 7 for Murray.

4. ESTIMATION OF MATERIALS

4.1 Image analysis

One of the simplest methods to estimate materials in CT images is to measure mean CT-values of some objects directly from the images. This method is primitive but effective. However, it is difficult to apply this method in all the sliced images for a three-dimensional structure. We can recognize CT-values of materials as peaks of a histogram of CT-values in three-dimensional images. However, we cannot recognize peaks of materials even in $\log(N)$-histograms if the modes of the materials are extremely low. Moreover, the histogram does not

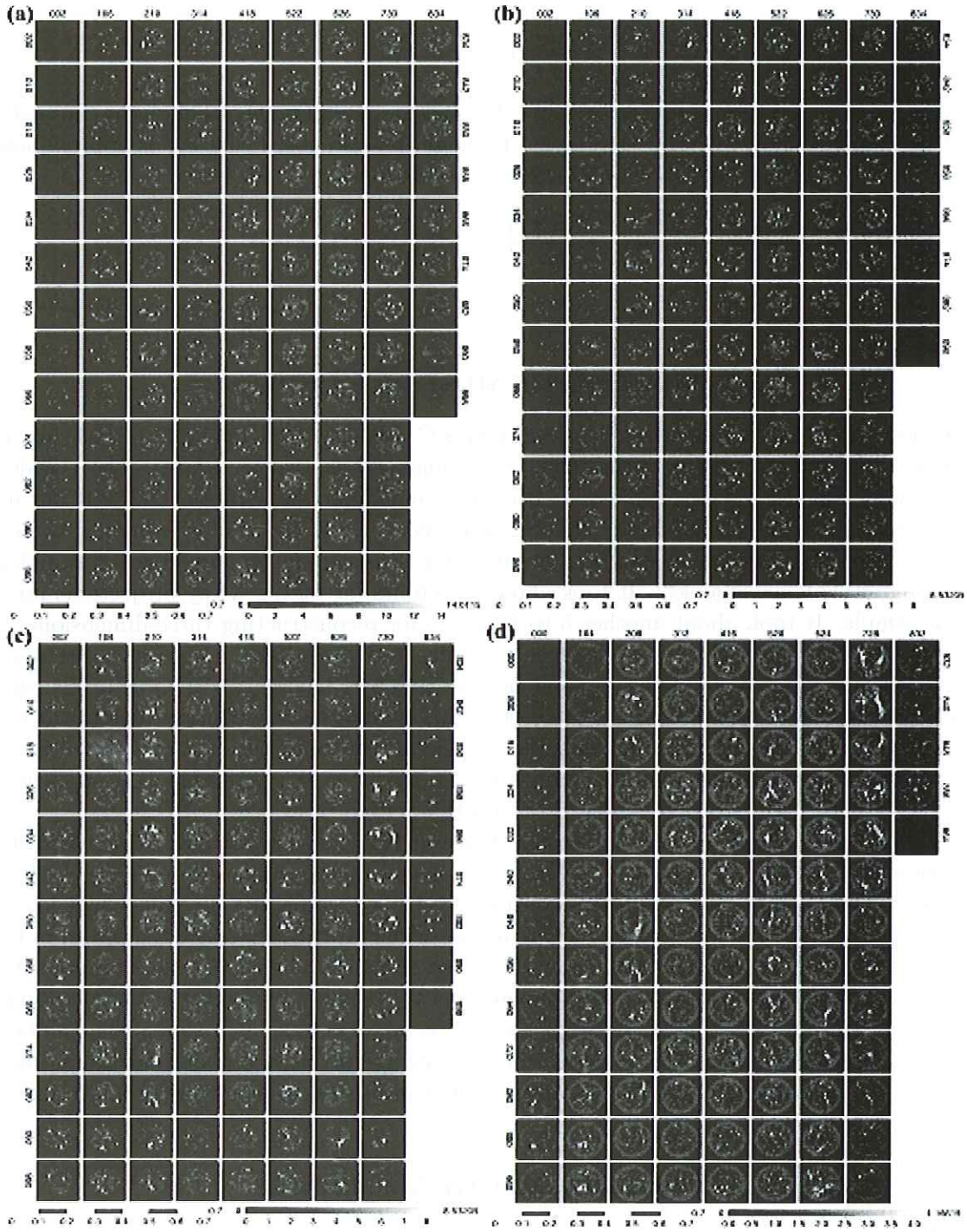

Fig. 2: Successive CT images of the analog samples. Images are shown in every 8 intervals. The length of a scale bar on the left bottom is 0.7 cm. A gray scale on the right bottom shows CT-values in cm^{-1}. (a) Analog ♯1 imaged at 25.0 keV. (b) Analog ♯1 imaged at 30.0 keV. (c) Analog ♯2 imaged at 30.0 keV. (d) Analog ♯2 imaged at 40.0 keV. Glass tubes (1.2 mm and 0.8 mm in outer and inner diameters, respectively) to hold the powder samples are seen.

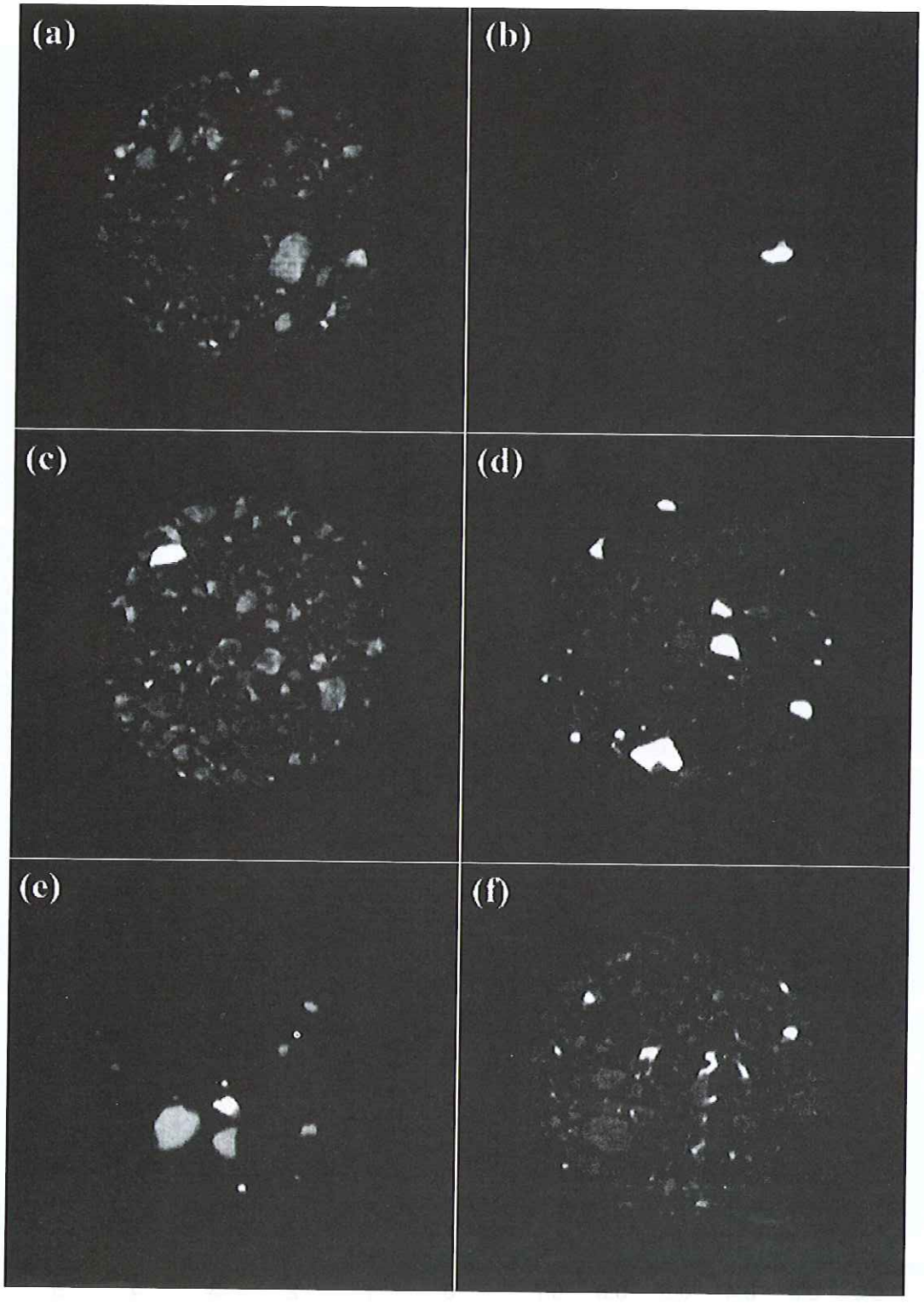

Fig. 3: Typical CT images of the analog samples. (a–c) Analog ♯1 imaged at 25.0 keV. (d–f) Analog ♯2 imaged at 30 keV. Ranges of CT-values are expressed as gray scale. The ranges are (a) 0–22.4 cm^{-1}, (b) 0–50.8cm^{-1}, (c) 0–22.4 cm^{-1}, (d) 0–14.8 cm^{-1}, (e) 0–29.8cm^{-1}, and (f) 0–14.8cm^{-1}. Glass tubes (1.2 mm and 0.8 mm in outer and inner diameters, respectively) to hold the powder samples are seen. The width of each image is 1.63 mm.

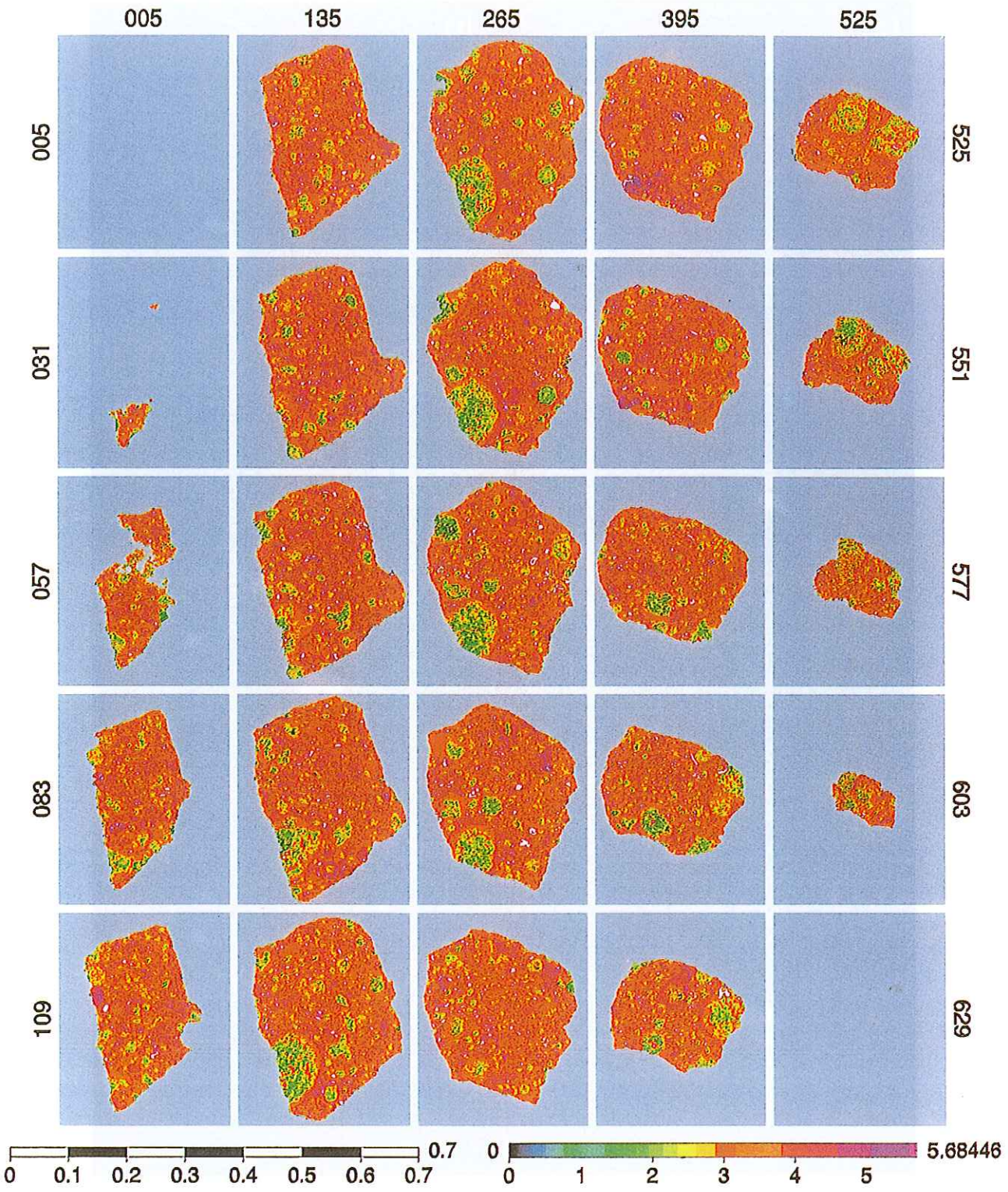

Fig. 4: Successive CT images of the Murray meteorite (CM2) imaged at 35.0 keV. Images are shown in every 26 intervals. The length of a scale bar on the left bottom is 0.7 cm. A gray scale on the right bottom shows CT-values in cm^{-1}.

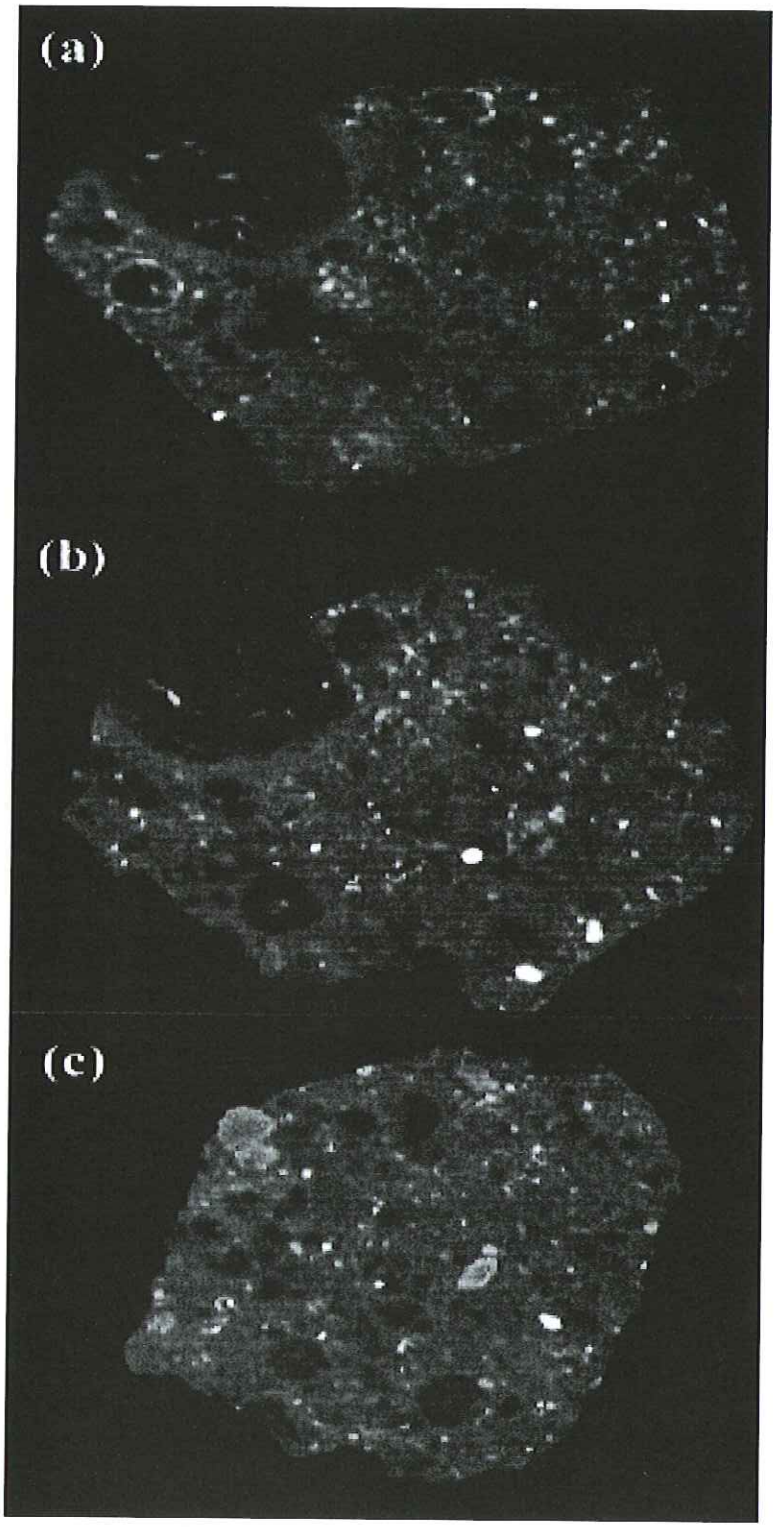

Fig. 5: Typical CT images of the Murray meteorite. Ranges of CT-values (0–8.63cm^{-1}) are expressed as gray scale. The width of each image is 3.69 mm. The images are rotated clockwise by 90 degrees from the image in Figure 4.

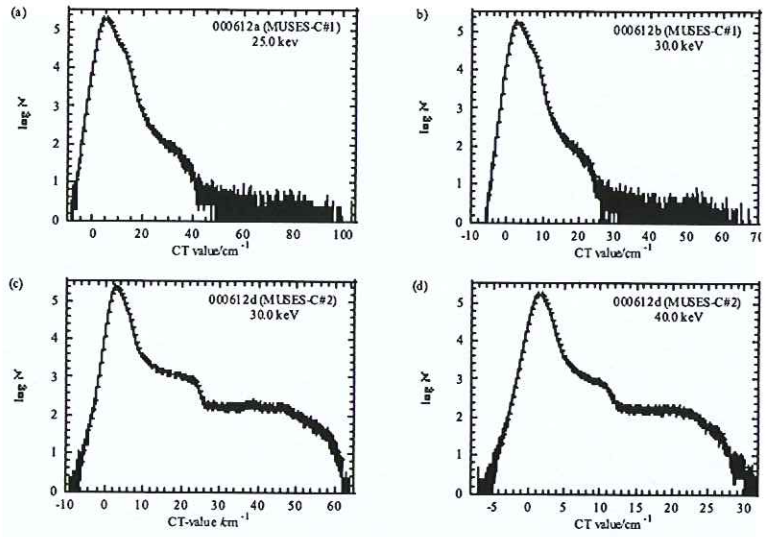

Fig. 6: Histograms of CT-values of the analog samples. The logarithm of the number of voxels is taken ($\log(N)$-histogram). (a) Analog ♯1 imaged at 25.0 keV. (b) Analog ♯1 imaged at 30.0 keV. (c) Analog ♯2 imaged at 30.0 keV. (d) Analog ♯2 imaged at 40.0 keV.

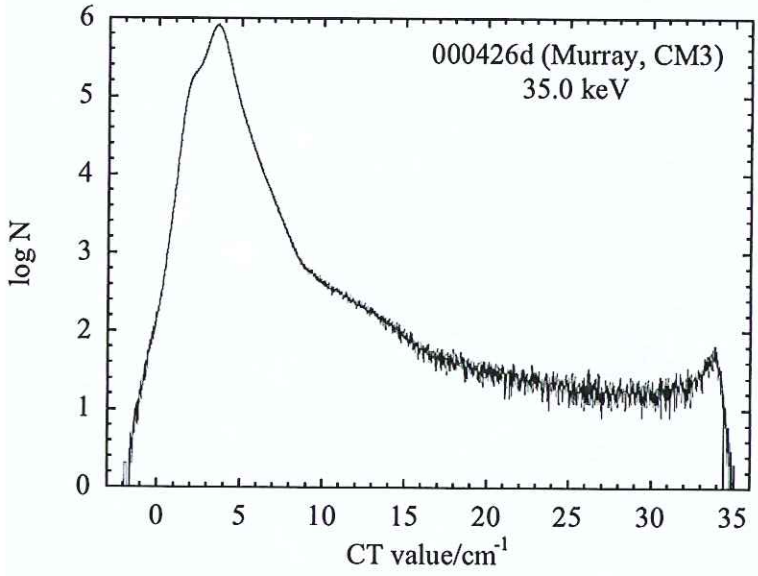

Fig. 7: A histogram of CT-values of the Murray meteorite. The logarithm of the number of voxels is taken ($\log(N)$-histogram).

include information of spatial distribution of materials. Accordingly, some peaks cannot be separated if the peak values resemble each other. To recognize CT-values of different materials systematically in three-dimensional images, we developed a new image analysis, named CBC-MS analysis. The procedure of the analysis is follows.

(1) Making images based on the logarithm of CT-values ($\log(N)$-images).

(2) Searching nearly homogeneous regions, which are larger than the spatial resolution and

have similar contrasts, in the $\log(N)$-images (cubic block check (CBC) analysis).

(3) Further searching nearly homogeneous regions in two types of CT images of the same sample taken at different photon energies by using photon energy dependence of LAC (multi-spectrum (MS) analysis).

In the analysis, we assume that the deviation of CT-value is proportional to the CT-value as Eq.(2). Accordingly, the $\log(N)$-images were used in the later analysis. The CBC analysis was made by introducing parameters named BS (block size) and PVD (pixel value difference). We check the homogeneity of a three-dimensional block with the size of $BS((2*BS+1)^3$ voxels; e.g., $3\times3\times3$ voxels for $BS=1$ and $5\times5\times5$ voxels for $BS=2$). If CT-values of all the voxels in a block belong to a given bin(s) of $log(N)$, the block is considered to be homogeneous (e.g., the voxels in the same bin are considered to be homogeneous for $PVD=0$, and the voxels in the neighbor bins are also considered to be homogeneous for $PVD=1$). We obtain histograms of voxels hitting the homogeneous criteria with different sets of BS and PVD in Tables 1 for the analog samples and Table 2 for Murray. In the MS analysis, voxels at the same location in CT images taken at different photon energies are compared. Histograms of voxels passing the CBC analysis at two different energies were made for the analog samples (Table 3).

4.2 Analog samples

LAC of the histogram peaks by the CBC-MS analysis (Tables 1 and 3) should correspond to those of nearly homogeneous materials. For the analog samples they are follows:

analog ♯1
material–1A: LAC=10.53–15.17 cm^{-1}(bins 47–48) at 25 keV
LAC=6.58–9.48 cm^{-1} (bins 47–48) at 30 keV
material–1B: LAC=31.45–37.74 cm^{-1}(bin 53) at 25 keV
material–1A: LAC=19.66-23.59 cm^{-1} (bin 53) at 30 keV
material–1C: probably LAC=78.26–93.91 cm^{-1} (bin 58) at 25 keV
probably LAC=48.91–58.70 cm^{-1} (bin 58) at 30 keV

analog ♯2
material–2A: LAC=5.49–6.58 cm^{-1} (bin 46) at 30 keV
LAC=2.74–3.29 cm^{-1} (bin 45) at 40 keV
material–2B: LAC=19.66–28.31cm^{-1} (bins 53–54) at 30 keV
LAC=9.83–11.79 cm^{-1} (bin52) at 40 keV
material–2C: LAC=33.97–48.91 cm^{-1} (bins 56–57) at 30 keV
LAC=16.98–24.46 cm^{-1} (bins 55–56) at 40 keV

In the both analog samples, the first peaks of the histograms (4.87 cm^{-1} at 25 keV and 2.78 cm^{-1} at 30 keV for ♯1, and 2.90 cm^{-1} at 30 keV and 1.51 cm^{-1} at 40 keV for ♯1: Fig. 6) do not hit the homogeneity criteria irrespective of the (BS, PVD) sets. Materials at the first peaks might be heterogeneous in the scale around or less than the size of the spatial resolution of the CT images. In order to estimate materials contained in the analog samples, the peak CT-values are compared with expected CT-values of some candidate minerals, which were calculated from their LAC and Eq.(1). In Fig. 8, the peak CT-values and the mineral CT-values at the two different photon energies are plotted. They are plotted almost on single lines (curves in a strict

bin ID j	LAC, 1 / cm 0.002000*(1+0.2)^j ~ 0.002000*(1+0.2)^(j+1)	pixels					
		PVD = 0			P VD = 1		
		BS = 1	BS = 2	BS = 3	BS = 1	BS = 2	BS = 3
37	1.701124 ~ 2.041349				1		
38	2.041349 ~ 2.449619				7		
39	2.449619 ~ 2.939543				58		
40	2.939543 ~ 3.527452				714		
41	3.527452 ~ 4.232942				6601		
42	4.232942 ~ 5.079531	1		3	4702	136	1
43	5.079531 ~ 6.095437	18			89841	717	10
44	6.095437 ~ 7.314524	62			117376	1289	6
45	7.314524 ~ 8.777429	170		1	16945	3169	117
46	8.777429 ~ 10.532915	528			145774	7096	120
47	10.532915 ~ 12.639497	4381	4		261354	36294	3394
48	12.639497 ~ 15.167397	10453	13		234680	35912	3487
49	15.167397 ~ 18.200876	718		4	6227	2908	67
50	18.200876 ~ 21.841052	47			5618	136	
51	21.841052 ~ 26.209262	11			1633	49	
52	26.209262 ~ 31.451114	18			1426	113	1
53	31.451114 ~ 37.741337	201		1	560	188	
54	37.741337 ~ 45.289605	6		3	44	6	
55	45.289605 ~ 54.347525				10		
56	54.347525 ~ 65.217031				8		
57	65.217031 ~ 78.260437				27		
58	78.260437 ~ 93.912524	3		1	11	2	
59	93.912524 ~ 112.695029	3		4	1		

000612b (30 keV) / MUSES-C analog sample #1

bin ID j	LAC, 1 / cm 0.001250*(1+0.2)^j ~ 0.001250*(1+0.2)^(j+1)	pixels					
		PVD = 0			P VD = 1		
		BS = 1	BS = 2	BS = 3	BS = 1	BS = 2	BS = 3
39	1.531012 ~ 1.837214				5		
40	1.837214 ~ 2.204657				125		
41	2.204657 ~ 2.645589				1359		
42	2.645589 ~ 3.174707				8557	1	
43	3.174707 ~ 3.809648				26434	79	
44	3.809648 ~ 4.571577	12			44948	246	
45	4.571577 ~ 5.485893	21			60374	761	1
46	5.485893 ~ 6.583072	156		1	12252	4484	85
47	6.583072 ~ 7.899686	1275			209473	22748	1456
48	7.899686 ~ 9.479623	3239			166229	19293	1370
49	9.479623 ~ 11.375548	306			31575	1249	12
50	11.375548 ~ 13.650657	6		3	722	20	
51	13.650657 ~ 16.380789	34			1399	58	
52	16.380789 ~ 19.656946	41			1484	177	5
53	19.656946 ~ 23.588336	158		1	449	162	
54	23.588336 ~ 28.306003				118		
55	28.306003 ~ 33.967203				10		
56	33.967203 ~ 40.760644				5		
57	40.760644 ~ 48.912773				9		
58	48.912773 ~ 58.695327	12			102	3	
59	58.695327 ~ 70.434393	9		5	7		

Table 1a: Results of CBC analysis for analog #1 at 25 keV (top) and 30 keV (bottom). parameters: $(BS, PVD) = (1,0), (2,0), (3,0), (1,1), (2,1)$ and (3,1).

bin ID j	LAC, 1 / cm 0.001250*(1+0.2)^j ~ 0.001250*(1+0.2)^(j+1)	pixels					
		PVD = 0			PVD = 1		
		BS = 1	BS = 2	BS = 3	BS = 1	BS = 2	BS = 3
39	1.531012 ~ 1.837214		8				
40	1.837214 ~ 2.204657		1		70		
41	2.204657 ~ 2.645589		2		532		
42	2.645589 ~ 3.174707		1		4380		
43	3.174707 ~ 3.809648		3		6617	5	
44	3.809648 ~ 4.571577	14		6	3110	698	3
45	4.571577 ~ 5.485893	197			124637	6201	236
46	5.485893 ~ 6.583072	1137		1	55400	17359	2074
47	6.583072 ~ 7.899686	417			65761	3623	66
48	7.899686 ~ 9.479623	17		3	768	19	
49	9.479623 ~ 11.375548				250		
50	11.375548 ~ 13.650657				233		
51	13.650657 ~ 16.380789	10			2008	308	33
52	16.380789 ~ 19.656946	800	13		9258	1526	236
53	19.656946 ~ 23.588336	3484	100		26604	6072	1446
54	23.588336 ~ 28.306003	931	10		9943	2286	379
55	28.306003 ~ 33.967203	64			1044	108	
56	33.967203 ~ 40.760644	2608	506	4	7440	2938	850
57	40.760644 ~ 48.912773	3226	282	1	11653	2803	371
58	48.912773 ~ 58.695327	1628	6		8090	965	28
59	58.695327 ~ 70.434393	50			856	156	1

000612d (40 keV) / MUSES-C analog sample #2

bin ID j	LAC, 1 / cm 0.000750*(1+0.2)^j ~ 0.000750*(1+0.2)^(j+1)	pixels					
		PVD = 0			P VD = 1		
		BS = 1	BS = 2	BS = 3	BS = 1	BS = 2	BS = 3
39	0.918607 ~ 1.102329		2				
40	1.102329 ~ 1.322794		2		8		
41	1.322794 ~ 1.587353		3		94		
42	1.587353 ~ 1.904824		2		455		
43	1.904824 ~ 2.285789		8		491		
44	2.285789 ~ 2.742946		2		3777	20	
45	2.742946 ~ 3.291536	12		4	0918	988	37
46	3.291536 ~ 3.949843	10		1	9864	109	
47	3.949843 ~ 4.739812	2			2938		
48	4.739812 ~ 5.687774		8		94	1	
49	5.687774 ~ 6.825329		1		673	35	
50	6.825329 ~ 8.190394	3			3378	177	18
51	8.190394 ~ 9.828473	191			12995	1827	130
52	9.828473 ~ 11.794168	2441	66		19114	4404	711
53	11.794168 ~ 14.153001	2		1	205	15	
54	14.153001 ~ 16.983602	34			2119	126	
55	16.983602 ~ 20.380322	708	1		8019	2487	524
56	20.380322 ~ 24.456386	2344	116		11850	2584	285
57	24.456386 ~ 29.347664	670	15		3969	409	6
58	29.347664 ~ 35.217196	4		2	46	23	

Table 1b: Results of CBC analysis for analog #2 at 30 keV (top) and 40 keV (bottom). parameters: $(BS, PVD) = (1,0), (2,0), (3,0), (1,1), (2,1)$ and (3,1).

rgb/000426d : error in LAC / LAC = 0.1

pixel value	range of LAC, 1 / cm	pixels						
		non-CBC	PVD = 1			P	VD = 0	
			BS = 1	BS = 2	BS = 3	BS = 1	BS = 2	BS = 3
0	pixels with too small LAC (ignored)							
1	0.022292 ~	209						
2	0.044584 ~	165						
3	0.066876 ~	205						
4	0.089168 ~	204						
5	0.111460 ~	167						
6	0.133752 ~	210						
7	0.156044 ~	204						
8	0.178336 ~	165						
9	0.200628 ~	207						
10	0.222920 ~	213						
11	0.245212 ~	385						
12	0.289796 ~	208						
13	0.312088 ~	213						
14	0.334380 ~	396						
15	0.378964 ~	400						
16	0.423548 ~	433						
17	0.468132 ~	412						
18	0.512716 ~	470						
19	0.557300 ~	673						
20	0.624176 ~	469						
21	0.668760 ~	1031						
22	0.757928 ~	836						
23	0.824804 ~	1250						
24	0.913972 ~	1415						
25	1.003140 ~	1750	4					
26	1.092308 ~	2964	4					
27	1.203768 ~	5187	39					
28	1.337520 ~	8923	199	1				
29	1.471272 ~	14832	1184	21		2		
30	1.605024 ~	32248	4751	241	14	63		
31	1.783360 ~	50570	11827	1136	131	129		
32	1.961696 ~	74970	18428	1705	110	364		
33	2.162324 ~	88334	24207	2303	163	262		
34	2.362952 ~	123369	35659	3305	320	711		
35	2.608164 ~	174935	64495	8803	1071	1565	4	
36	2.875668 ~	282877	136949	25851	4724	4095	27	
37	3.165464 ~	461581	281607	80397	20359	12087	116	
38	3.477552 ~	573927	401992	152860	50996	21896	393	5
39	3.811932 ~	490246	324919	105194	29365	22335	454	18
40	4.213188 ~	230321	134680	32109	7954	4778	61	1
41	4.614444 ~	114084	49365	7996	1631	1942	13	
42	5.082576 ~	57193	10822	939	69	978	16	
43	5.595292 ~	6354						
44	5.684460 ~	pixels with too large LAC (ignored)						
255	pixels outside the sample (ignored)							

Table 2: Results of CBC analysis for Murray at 35 keV. Parameters: $(BS, PVD) = (1,0), (2,0), (3,0), (1,1), (2,1)$ and (3,1). CT-values larger than 5.68 cm^{-1} are not analyzed.

000612a and 000612b : PVD = 0 / BS = 1

	44	45	46	47	48	49	50	51	52	53	54	55	56	57	58	59
44	1	1														
45																
46			6	1												
47				80	6											
48					746											
49						35										
50																
51								2								
52									5							
53										16	1					
54																
55																
56																
57																
58															2	
59																3

000612a and 000612b : PVD = 0 / BS = 2 ... no pixel.

000612a and 000612b : PVD = 0 / BS = 3 ... no pixel.

000612a and 000612b : PVD = 1 / BS = 1

	40	41	42	43	44	45	46	47	48	49	50	51	52	53	54	55	56	57	58	59
40	2	1	1																	
41	1	60	119	28	1															
42	2	85	772	908	104															
43		22	762	4289	2915	204	3													
44			56	2275	9996	5167	260	1												
45				97	3094	16677	10117	785	11											
46					46	4077	35062	31687	2025	2										
47						44	6606	97794	53983	335	1									
48							28	13729	#####	14767	15									
49								12	5180	17868	1519	1								
50									1	374	1886	244								
51											38	657	273	1						
52												39	690	393						
53													12	872	227					
54														2	71					
55																1	3			
56																	2			
57																	1	5		
58																		8	65	
59																			16	35

000612a and 000612b : PVD = 1 / BS = 2

	43	44	45	46	47	48	49	50	51	52	53	54	55	56	57	58
43	15	2														
44	2	46	5													
45			201	53												
46			5	1034	958	25										
47				34	9677	3827	8									
48					536	12240	600									
49						56	588	33								
50							1	7								
51									17	8						
52									1	52	39					
53											80	3				
54																
55																
56																
57																
58																1

000612a and 000612b : PVD = 1 / BS = 3

	46	47	48	49
46	6	15		
47		563	107	
48		10	847	2
49				2

Table 3a: Results of MS analysis for analog #1 at 25 keV (top) and 30 keV (bottom). Parameters: $(BS, PVD) = (1,0), (2,0), (3,0), (1,1), (2,1)$ and (3,1).

000612c and 000612d : PVD = 0 / BS = 1

	47	48	49	50	51	52	53	54	55	56	57	58	59
46	1												
47													
48													
49													
50						1							
51						5	79						
52							109	255					
53								2					
54									7				
55										263	101	78	
56										69	1247	137	
57												249	28
58													3

000612c and 000612d : PVD = 0 / BS = 2

	53	54	55	56	57
52	1				
53					
54					
55					
56					78

000612c and 000612d : PVD = 0 / BS = 3 ... no pixel.

000612c and 000612d : PVD = 1 / BS = 1

	41	42	43	44	45	46	47	48	49	50	51	52	53	54	55	56	57	58	59
40	1	1	1																
41	1	6	16	2															
42	1	19	57	118	48	2													
43		9	101	715	1096	226	5												
44			31	722	4730	4822	629	1											
45			2	134	2978	15317	7224	83											
46				5	228	4610	7595	504	6										
47				1	2	156	872	364	16		2	3							
48						2	24	67	13	7	18	108	6						
49							1	15	6	9	88	551	191						
50										2	241	1171	728	1					
51											29	1781	8173	641					
52												532	9634	7646	3				
53												3	143	692	111	34			
54															478	690	221	6	
55															83	3888	2310	799	
56																1681	6417	2805	7
57																	324	2979	557
58																		14	230

000612c and 000612d : PVD = 1 / BS = 2

	45	46	47	48	49	50	51	52	53	54	55	56	57	58	59
44	2	1													
45	4	514	127												
46		13	51												
47															
48															
49								12							
50							8	108	3						
51								244	1088	132					
52								64	2066	1824					
53										15					
54											32	38	8		
55											7	1593	352	180	
56												660	1547	175	
57													33	251	106
58														4	19

000612c and 000612d : PVD = 1 / BS = 3

	46	47	48	49	50	51	52	53	54	55	56	57	58
45	28												
46													
47													
48													
49													
50							7						
51								61	8				
52							1	349	282				
53													
54													
55											403	8	2
56											53	221	
57												3	2

Table 3b: Results of MS analysis for analog #2 at 30 keV (top) and 40 keV (bottom). Parameters: $(BS, PVD) = (1,0), (2,0), (3,0), (1,1), (2,1)$ and (3,1).

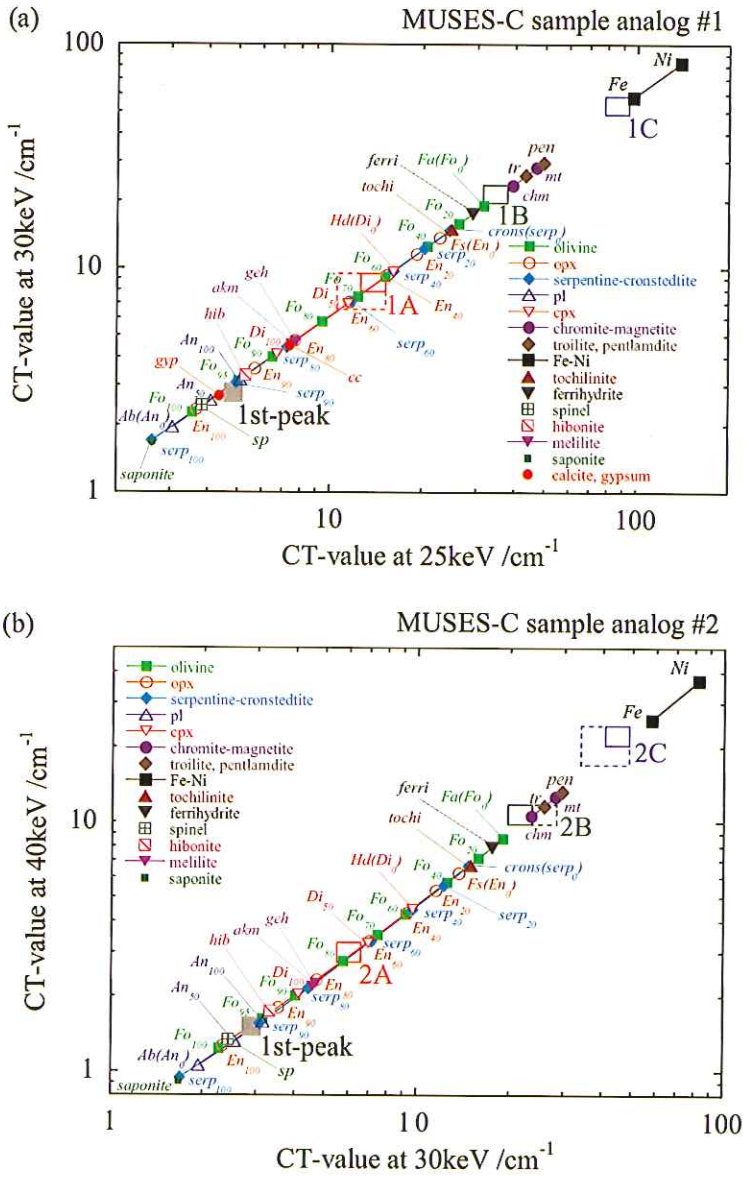

Fig. 8: CT-values of materials in the analog samples at different photon energies. The CT-values were obtained by an image analysis (CBC-MS analysis) and from peaks of the CT-value histograms. CT-values of some minerals calculated from their LAC and the CT-value - LAC relation in Eq.(1) are also shown for comparison. (a) Analog ♯1. (b) Analog ♯2.

sense), suggesting that imaging of a sample at different photon energies are not necessary for the estimation of material by using LAC at least in the range of the photon energies used in the present study. Because the information of LAC is one-dimensional and the ranges of LAC by the Mg-Fe substitution of ferromagnesian silicates, such as olivine, are wide, we cannot distinguish many silicate, oxide, carbonate and sulfate minerals. Furthermore, contribution of voids to the CT-values is also possible for the first peak materials. Based on the present results (Fig. 8), we can mention the following possibilities:

analog ♯1
first peak–1: Fe-bearing hydrous silicates, such as serpentine (Mg♯ ∼ 0.9),
Mg-rich ferromagnesian silicate, such as olivine (∼Fo95),
Ca-rich plagioclase,
mixtures of above minerals,
or void + fine-grained Fe-rich hydrous and/or ferromagnesian silicates like matrix of chondrites (this is most probable)
material–1A: Fe-rich ferromagnesian and/or hydrous silicates, such as olivine (Fo_{60}-Fo_{70}) and serpentine (50% serpentine–50% cronstedtite)
possibilities of plagioclase, highly refractory minerals (melilite, hibonite and spinel), calcite and gypsum can be excluded
material–1B: Fe-sulfides (troilite or pentlandite),
or Fe-oxides (magnetite) or chromite
material–1C: (Fe-Ni) metal

analog ♯2
first peak–2: Fe-bearing hydrous silicates, such as serpentine (Mg♯ ∼ 0.9),
Mg-rich ferromagnesian silicate, such as olivine ($\sim Fo_{95}$),
Ca-rich plagioclase,
mixtures of above minerals,
or void + fine-grained Fe-rich hydrous and/or ferromagnesian silicates like matrix of chondrites (this is most probable)
material–2A: Ferromagnesian and/or hydrous silicates, such as olivine (Fo_{75}-Fo_{80}) and serpentine (60–70% serpentine-40–30% cronstedtite)
possibilities of plagioclase, highly refractory minerals (melilite, hibonite and spinel), calcite and gypsum can be excluded
material–2B: Fe-sulfides (troilite or pentlandite),
or Fe-oxides (magnetite) or chromite
material–2C: Fe-Ni metal (may be partially oxydized or associated with some Fe sulfides)
After the imaging, the analog samples were observed under a binocular optical microscope.

analog ♯1
fine–1: very fine dark gray particles (some portions are gray) (common)
grain-1a colorless grains (common)
grain-1b bronzy grains (rare)

analog ♯2
fine-2: fine white gray particles (common)
grain-1a gray-colorless grains (common)
(yellow stuff is attached to the surfaces of some grains)
grain-1b bronzy grains (a few)

For analog ♯1, first peak-1, material-1A and material-1B in the CT images must correspond to fine-1, grain-1a and grain-1b, respectively. First peak-1 might be matrix of a carbonaceous chondrite. Material-1A might be olivine or pyroxene. Material-1B might be troilite or pentlandite. For analog ♯2, first peak-2 and material-2A in the CT images must correspond to fine-2 and grain-2a, respectively. First peak-2 might be finely milled minerals, such as Mg-rich olivine, Mg-rich orthopyroxene and/or Ca-rich plagioclase. Material-2A might be olivine or

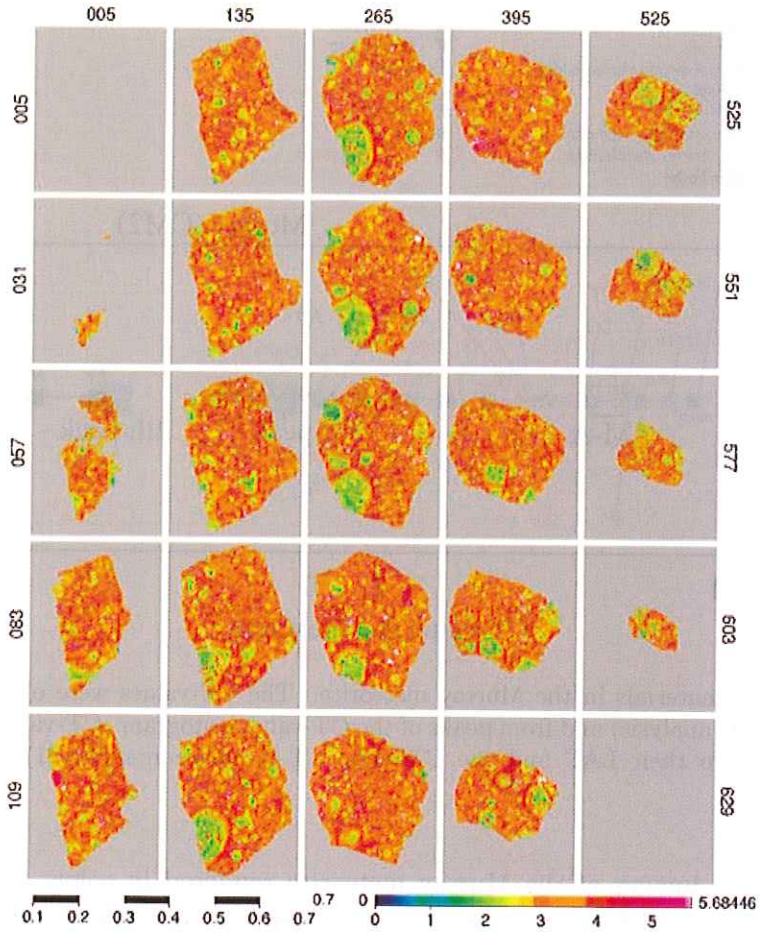

Fig. 9: CT-images of the Murray meteorite rendered in color (the same slices as Figure 4). Each bin of the CT-values is determined by CBC analysis and expressed as the logarithm of the CT-value ($\log(f)$-image). The length of a scale bar on the left bottom is 0.7 cm. A color scale on the right bottom shows CT-values in cm^{-1}.

pyroxene. Material-2B and probably material-2C corresponds to grain-1b. Material-2B might be troilite or pentlandite, and material-2C might be mixtures of Fe-Ni metal and Fe sulfides.

4.3 Murray meteorite

MS analysis was not made for this sample because the imaging was done only at 35.0 keV. Two peaks were detected by the CBC analysis (Table 2):

material-MA: LAC=1.78–2.16 cm^{-1} (bins 31–32)
material-MB: LAC=3.48–4.21 cm^{-1} (bins 38–39)

Material-MA is indicated by a week peak in the CBC analysis (Table 2), which corresponds to a bump in the histogram at 2.10 cm^{-1} (Fig. 7). Material-MB is indicated by a major peak (Table 2), which corresponds to a peak at 3.55 cm^{-1} (Fig. 7). In this analysis, CT-values larger than 5.68 cm^{-1} were not considered. In stead, a bump at about 13 cm^{-1} (third peak) and a peak at 33.9 cm^{-1} (fourth peak) in the histogram (Fig. 7) are also taken into consideration.

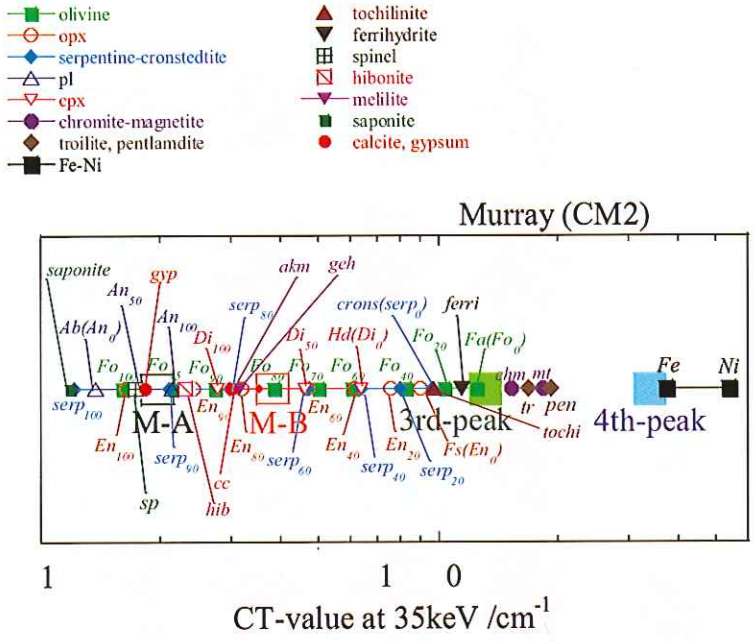

Fig. 10: CT-values of materials in the Murray meteorite. The CT-values were obtained by an image analysis (CBC analysis) and from peaks of the CT-value histogram. CT-values of some minerals calculated from their LAC and the CT-value - LAC relation in Eq.(1) are also shown for comparison.

Fig. 9 shows $\log(f)$ images of the Murray meteorite rendered in color. Materials-MA and -MB are expressed by yellowish green and orange, respectively. Third and fourth peaks are expressed as white. It is seen from Fig. 9 that most of chondrules correspond to material-MA and matrix to material-MB. The peak CT-values are compared with mineral CT-values in Fig. 10. Material-MA can be explained by Mg-rich olivine (Fo_{95}- Fo_{98}). This is consistent with the composition of majority of chondrule olivine in CM chondrites (>Fo_{95}) (Brealey & Jones, 1998). Material-MB can be explained by Fe-rich hydrous silicate, such as 70% serpentine - 30% cronstedtite, or more Fe-rich serpentine and pores. This is also consistent with serpentines in the matrix of the Murray meteorite (20–30% serpentine - 80–70% cronstedtite: Brealey & Jones, 1998) if porosity of the matrix is taken into consideration. The CT-value of third peak should indicate tochilinite and/or Fe sulfides. PCP's are represented by third peak. Fourth peak should correspond to Fe-Ni metals or their altered products.

4.4 Applicability of CT-values for estimating materials in MUSES-C samples

The results on the analog samples show that we can estimate mineral candidates in an unknown sample by using CT-value histogram and CBC analysis. The consistency of the CT-values in the images with mineralogy of Murray strongly suggests that we can recognize most of mineral phases in CT images if the constituent minerals are known by an SEM/EPMA observation.

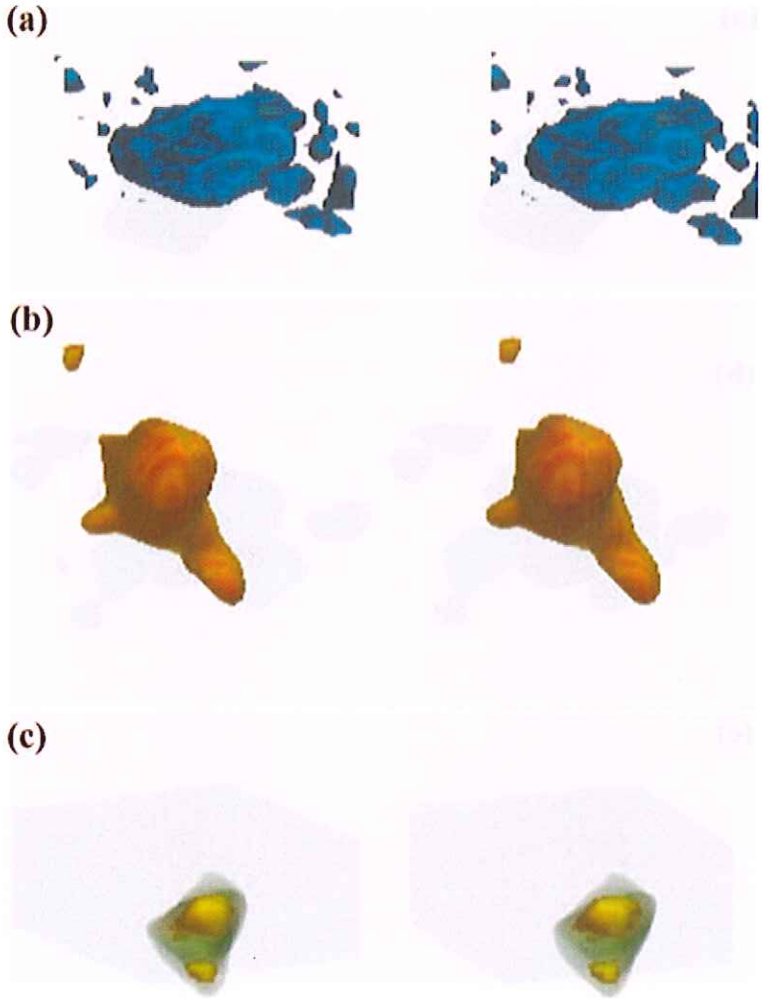

Fig. 11: Stereographs of grains in analog ♯1. (a) A grain of ferromagnesian silicate(?) of about 190 μm in length. (b) A grain of Fe-Ni metal(?) of about 50–80 μm in length. (c) A grain of Fe sulfide(?) of about 70 μm in length. The images are rendered in color. See text for more details.

5. TREE-DIMENSIONAL OBSERVAION

5.1 Analog samples

Stereographs of some grains are shown in Fig. 11 for analog ♯1. A grain in Fig. 11a, where material with LAC $>$ 12cm^{-1} are shown, is the largest grain in Fig. 3a (bright rectangular grain in a slightly lower right portion from the center). The size is about 130–190 μm. The CT-value is about 15 (12–17) cm^{-1}, which corresponds to material-1A (ferromagnesian silicate grain?). A grain in Fig. 11b, where material with LAC $>$ 35 cm^{-1} are shown, is the brightest grain in Fig. 3b (grain in a slightly lower right portion from the center). The size is about 50–130 μm. The CT-value in the brightest part is about 85 (80–92) cm^{-1}, which corresponds to material-1C (Fe-Ni metal?) and that in bright part (upper right part of the grain in Fig. 3b) is about 39 cm^{-1}, which corresponds to material-1B (Fe sulfide?). A grain in Fig. 11c, where material with LAC$>$35 cm^{-1} are shown as solids and with 21$<$LAC$<$35 cm^{-1} as transparent,

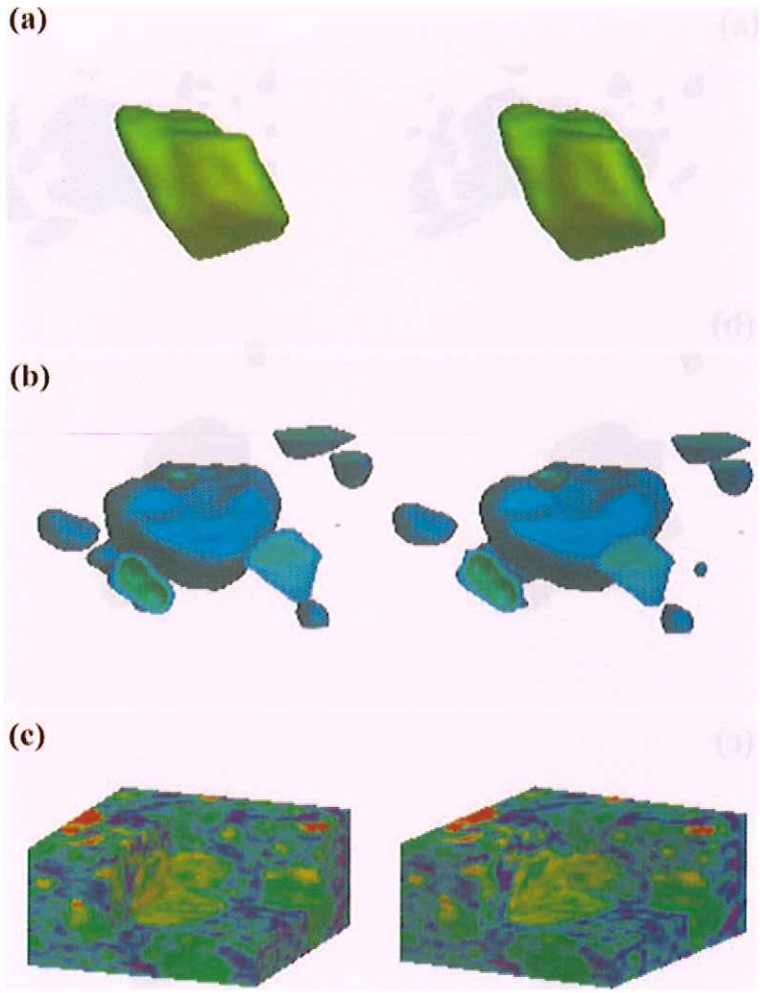

Fig. 12: Stereographs of grains in analog ♯2. (a) A grain of Fe-Ni metal(?) of about 120 μm in length. (b) A grain of Fe sulfide(?) of about 180 μm in length. (c) A grain of ferromagnesian silicate(?) of about 140–180 μm in length, located at the center of the figure. The images are rendered in color. See text for more details.

is the brightest grain in Fig. 3c (grain in a left upper portion from the center). The size is about 70–120 μm. The CT-value is about 30 (23–38) cm^{-1}, which corresponds to material-1B (Fe sulfide?).

Stereogrphs of some grains are shown in Fig. 12 for analog ♯2. A grain in Fig. 12a, where material with LAC>35 cm$^-$1 are shown, is the largest grain in Fig. 3d (bright grain near the bottom). The size is about 120–130 μm. The CT-value is about 48 (42–53) cm^{-1}, which corresponds to material-2C (Fe-Ni metal grain?). A grain in Fig. 12b, where material with 15<LAC<28cm^{-1} are shown, is the largest grain in Fig. 3e (bright grain in a lower right portion). The size is about 140–180 μm. The CT-value is about 24 (22–25) cm^{-1}, which corresponds to material-2B (Fe sulfide grain?). A yellow-green grain in the center of Fig. 12c is the largest grain in Fig. 3f (bright grain in a lower left portion). The size is about 140–180 μm. The CT-value is about 5.9 (4.7–7.8) cm^{-1}, which corresponds to material-2A (ferromagnesian silicate grain?). The sizes of large grains are about 100 μm (up to about 200 μm) in the both samples. The sizes of small grains are less than the spatial resolution of the CT images (about

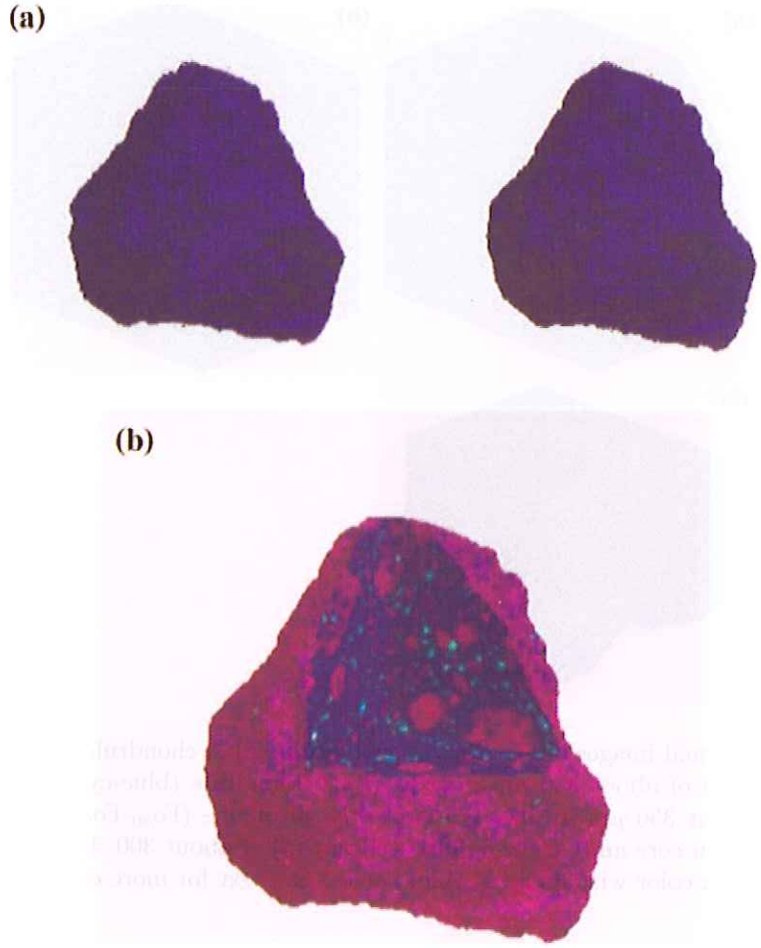

Fig. 13: Three-dimensional image of the Murray meteorite. (a) A stereograph. (b) A cut image. The height of the sample is about 4 mm. The images are rendered in color with different color tables.

10 μm). In principle, size distribution of grains with different CT-values can be obtained from three-dimensional images of powders. In the present study, however, we did not obtain size distribution due to the presence of grains smaller than the spatial resolution. Some grains have structures due to their heterogeneity (e.g., a dark grain partly surrounded by slightly bright rim in a right top portion of Fig. 3a). Three-dimensional structure of each grain did not investigated in the present study because of the poor spatial resolution compared with the grain size. However, if the high spatial resolution detector system is used (the spatial resolution is about 1 μm: Uesugi et al., 2000), three-dimensional structures of large grains (about 100 μm) can be examined.

5.2 Murray meteorite

Stereographs of a whole sample of the Murray meteorite are shown in Fig. 13. Stereographs of each chondrule and mineral fragment are also shown in Fig. 14. Fig. 14a shows a chondrule in the bottom of Fig. 5a. The size of the chondrule is about 350 μm. Dark material inside the chondrule has CT-value of about 2.2 (1.4–3.2) cm^{-1}, which corresponds to material-MA

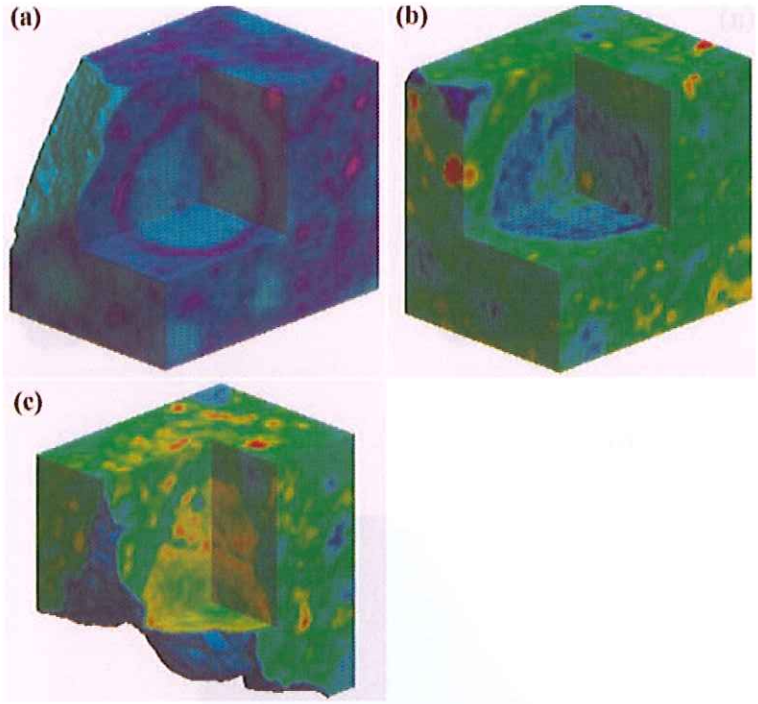

Fig. 14: Three-dimensional images in the Murray meteorite. (a) A chondrule (cyan) with FeO-rich rim (blue-magenta) of about 350 μm in size. (b) A chondrule (blue-cyan, yellowish green in the center) of about 350 μm in size. (c) Probably an olivine (Fo_{80}-Fo_{60} from core to rim) grain (yellowish green core and yellow-reddish yellow rim) of about 300–400 μm in size. The images are rendered in color with different color tables. See text for more details.

($Fo_{85--100}$ olivine). The bright rim has CT-value of about 7 cm^{-1}, which corresponds, to Fe-rich silicates. Fig. 14b shows a chondrule in a lower right portion of Fig. 5b. The size of the chondrule is about 350 μm. Dark material inside the chondrule has CT-value of about 1.9 (1.4–2.9) cm^{-1}, which corresponds to material-MA ($Fo_{90--100}$ olivine). The bright part at the center has CT-value of about 4–5 cm^{-1}indicating Fe-rich mafic minerals (about Fo_{70--80} if they are olivine). Fig. 14c shows a mineral grain in the left bottom of Fig. 5c. The size of the grain is about 300–400 μm. The CT-value is about 5.1 (4.1–6.3) cm^{-1}. This grain does not correspond to any material of MA and MB probably because of its low population. If it is olivine, the composition changes from $\sim Fo_{80}$ (core) to $\sim Fo_{60}$ (rim).

6. CONCLUSION

(1) Two MUSES-C analog samples (♯1 and ♯2) were imaged three-dimensionally without breaking the samples by an X-ray CT system at SPring-8 with the spatial resolution of about 10 μm. Because the samples are fine powders, which are not suitable for texture observation of a bulk sample, we also imaged a piece of a CM2 meteorite (the Murray meteorite).

(2) We imaged standard minerals before imaging the analog samples to compare the CT-values, f, of materials in CT images with their X-ray linear attenuation coefficient (LAC), μ. We obtained the quantitative relation between them: $f = 0.9\ \mu$(Fig. 1). By using this relation, we can estimate materials from their CT-values even if samples are powder.

(3) We developed a new image analysis, named CBC (cubic block check)-MS (multi-spectrum) analysis. By using this method, we looked for nearly homogeneous portions three-dimensionally (Tables 1–3). Some peaks of the histograms of CT-values (Figs. 6–7) correspond to the materials detected by the CBC-MS analysis. However, some other peaks do not correspond to the materials determined by the CBC-MS analysis. This is probably because the grain sizes are so small compared with the spatial resolution that the CBC-MS analysis cannot detect some materials.

(4) Minerals in the imaged samples were estimated from the CT-values of the materials determined by the CBC-MS analysis and the histogram peaks (Figs. 8 and 10). We can estimate only mineral candidates for the analog samples (see Table in chapter 4.2) because the LAC-value ranges by Mg-Fe substitution in ferromagnesian silicate minerals are wide. The most probable materials are hydrous and/or anhydrous Mg-Fe silicates like the matrix of carbonaceous chondrites, Fe-rich ferromagnesian silicates, such as olivine, Fe sulfide and Fe-Ni metal in the analog sample ♯1. Similar minerals should be present in analog ♯2, but the Fe-rich ferromagnesian silicates are more Mg-rich than that in analog ♯1.

(5) The CT-values in the images of Murray are consistent with its mineralogy (Mg-rich olivine in chondrules, Fe-rich serpentine in matrix and tochilinite in PCP's.) This strongly suggests that we can recognize most of mineral phases in CT images if the constituent minerals are known by an SEM/EPMA observation.

(6) We can observe three-dimensional structures of the samples (Figs. 11–14). We can recognize chondrules and mineral grains in Murray (Fig.14). If the high spatial resolution detector system (about 1 μm: Uesugi et al., 2000) is used, three-dimensional structures of large grains (about 100 μm) in the analog samples can be examined.

(7) In summary, the present method can be useful to describe three-dimensional textures of unknown samples without breaking samples by using CT-values. We believe that curation of MUSES-C samples will be made effectively by using the present method.

REFERENCES

Brearley A. J. & Jones R. H., 2000, *Chondritic Meteorites, in "Planetary Materials" ed. J. J. Papike* **3-1 - 3-398**, Mineralogical Society of America.

Tsuchiyama A., Hanamoto T., Nakashima Y. & Nakano T., 2000,Quantitative evaluation of attenuation contrast of minerals by using a medical scanner. *Jour. Mineral. Petorl. Sci* **95**, 125–137.

Uesugi K., Tsuchiyama A., Nakano T., Suzuki Y., Yagi N., Umetani K. & Kohmura Y., 1999, Development of micro-tomography imaging system for rocks and mineral samples. In "Developments in X-ray Tomography II", *Ed. U. Bonse, Proc. SPIE* **3772**, 214–22.

Uesugi K, Suzuki Y., Yagi N., Tsuchiyama A., & Nakano T., 2000, Development of high spatial resolution X-ray CT system for rocks and mineral samples *Proceedings of Nuclear Instruments and Methods, Sec. A,* **467–468**, 853–856.

List of Authors and Coauthors

EBIHARA, Mitsuru	Tokyo Metropolitan University
FUJIWARA, Akira	The Institute of Space and Astronautical Science
HIDAKA, Hiroshi	Hiroshima University
IKEDA, Eiji	Kyushu University
KOBAYASHI, Katsura	Okayama University
KOMIYA, Masayoshi	National Institute of Advanced Industrial Science and Technology
KURITANI, Takeshi	Okayama University
KUSHIRO, Ikuo	The Institute for Frontier Research on Earth Evolution
MAKISHIMA, Akio	Okayama University
MITA, Hajime	University of Tsukuba
MIURA, Yayoi N.	University of Tokyo
MURAE, Tatsushi	Kyushu University
MORIGUCHI, Takuya	Okayama University
NAGAO, Keisuke	University of Tokyo
NAKAMURA, Eizo	Okayama University
NAKAMURA, Tomoki	Kyushu University
NAKANO, Tsukasa	Geological Survey of Japan/AIST
NOGUCHI, Takaaki	Ibaraki University
NARAOKA, Hiroshi	Tokyo Metropolitan University
OKAZAKI, Ryuji	University of Tokyo
OSAWA, Takahito	University of Tokyo
OURA, Yasuji	Tokyo Metropolitan University
SAKAGUCHI, Chie	Okayama University
SHIMOYAMA, Akira	University of Tsukuba, Kochi Gakuin College
TAKEI, Hiroyuki	Okayama University
TANAKA, Ryoji	Okayama University
TSUCHIYAMA, Akira	Osaka University
UESUGI, Kentaro	SPring-8/JASRI
YANO, Hajime	The Institute of Space and Astronautical Science
YOKOYAMA, Tetsuya	Okayama University
YONEDA, Shigekazu	National Science Museum
ZOLENSKY, Michael E.	NASA Johnson Space Center